An Improved Pulse Density Modulation Strategy Based on Harmonics for ICPT System

Xuerui Sheng and Liming Shi, *Member, IEEE*

***Abstract*—To improve the efficiency of high frequency inverter (HFI) in inductively coupled power transfer system, pulse density modulation (PDM) is often used. However, the output current of the HFI fluctuates seriously, especially at light load. It affects the stable operation of the system and the implementation of zero voltage switching. In this article, an improved pulse density modulation (IPDM) is proposed to reduce current fluctuation. It applies harmonics pulse to replace the fundamental pulse and zero state, and evenly distributes the switching sequence to reduce current fluctuation. Simultaneously, the best phase-shift angle of harmonics is obtained by using the transient analysis method to further reduce the output current fluctuation. The IPDM current fluctuation is less than PDM and the efficiency become higher at light load by the theoretical analysis, while PDM is better at heavy load. So, a hybrid modulation strategy is applied that IPDM and PDM are used for light and heavy load, respectively. The experimental results show that the HFI output current ripple coefficient is reduced by 15% to 62% and the efficiency is improved at light load.**

***Index Terms*—Current fluctuation, improved pulse density modulation (IPDM), inductively coupled power transfer (ICPT), zero voltage switching (ZVS).**

I. Introduction

INDUCTIVELY coupled power transfer (ICPT) technology is a power supply method which can transfer electrical energy from a power supply side to a load side based on the principle of electromagnetic induction [1]–[5]. With the merit of safety and convenience, ICPT technology has been applied widely in electronic product charging [6], rail transit power supply [7]–[9], biomedical implants [10].

The ICPT system consists mainly of transmitter-side converter, coupled mechanism and receiver-side converter. In order to control the ICPT system efficiently and stably, two methods have been studied at present. One method regulates the output voltage by controllable rectifier [11] or dc–dc converter [12] on the pick-up side. Although the method is simple in control, the uncontrolled transmitting side may cause some problems, such as low system efficiency. Another method control high frequency inverter (HFI) [13], [14] to stabilize the output voltage and power by wireless communication.

Recently, there are many research results about the high-efficiency modulation strategies for HFI, such as frequency variation (FV), pulsewidth modulation (PWM), phase-shift variation (PS) and pulse density modulation (PDM).

In [15], FV method based on PLL is proposed to regulate the output voltage and power. It can achieve zero voltage switching (ZVS) at turn-ON, but it still suffers from hard switching at turn-OFF.

Conventional PWM control method regulating output voltage or power has been researched in [16], [17]. In [16], the variable switching frequency and duty cycle are proposed to adapt to changing conditions. The specific experimental analysis is performed at a fixed duty cycle and the HFI soft-switch problem was not considered. An adjustable frequency-duty-cycle hybrid control method was implemented in [18]. It is to greatly reduce the frequency change by changing the duty cycle. However, this method still has a large shutdown current and an increase in the harmonic ratio of the HFI output current when the duty cycle is small.

PS is the most common control strategy with fixed frequency and duty cycle for HFI [19], [20]. However, neither ZVS nor zero current switching (ZCS) can be achieved at turn-ON and turn-OFF for lagging bridge arms, and the harmonic content is large. As a result, the efficiency of the HFI is greatly reduced.

In order to realize ZVS or ZCS, a PDM method was proposed [21]–[23]. The basic idea of the PDM method is to regulate the output voltage by controlling the time it takes to transfer energy for a fixed period of time. Its advantage is that ZVS at turn-ON and quasi-ZCS at turn-OFF can be realized to minimize the switching losses of HFIs. However, conventional PDM can cause serious current fluctuation, even current discontinuity at light loads. This will affect the operation of the system and have a severe impact on the device. In addition, frequency tracking is difficult to implement when the current become discontinuous at light load. The factors that influence current fluctuation are the quality factor of the system and the pulse distribution of the PDM. When the parameters of the system are fixed, the current fluctuation can only be reduced by optimizing the pulse distribution of the PDM.

An improved pulse density modulation (IPDM) based on the combination of fundamental, harmonics, and zero state is proposed in this article. It is to replace the switching sequence composed of the fundamental wave and the zero state by using harmonics to obtain a more evenly distributed switching

Manuscript received July 6, 2019; revised September 28, 2019; accepted December 2, 2019. Date of publication December 6, 2019; date of current version March 13, 2020. This work was supported by the National Key R&D Program of China (2017YFB1201003-009). Recommended for publication by Associate Editor A. Safaee. *(Corresponding author: Liming Shi.)*

The authors are with the Key Laboratory of Power Electronics and Electric Drive, Institute of Electrical Engineering, Chinese Academy of Sciences, Beijing 100190, China, and also with the University of Chinese Academy of Sciences, Beijing 100049, China (e-mail: sxr@mail.iee.ac.cn; limings@mail.iee.ac.cn).

Color versions of one or more of the figures in this article are available online at http://ieeexplore.ieee.org.

Digital Object Identifier 10.1109/TPEL.2019.2958644

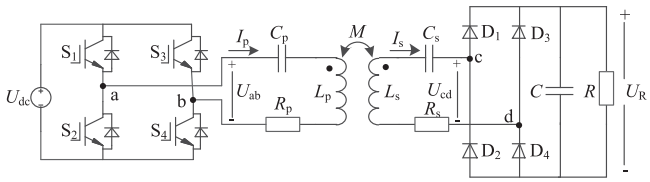

Fig. 1. Main circuit of ICPT system.

sequence at light load. For example, a switching sequence composed of one fundamental and two zero states can be replaced with a third harmonic. It reduces the HFI output current ripple by evenly distributing the pulses that transfer energy to the load throughout the switching cycle. And the efficiency is also improved at light load. Therefore, IPDM is suitable for light load and PDM can be used at heavy load.

II. Traditional PDM

In response to the low coupling coefficient and large leakage inductance problems, the series–series compensated topology is adopted to compensate the leakage inductance of the transmitting and pick-up coils in the article [24]. This topology is simple in structure and has a characteristic that the output current of the pick-up side is constant.

The main circuit diagram of the ICPT system is shown in Fig. 1. $U_{\rm dc}$ is the dc input voltages of the HFI, U_{ab} is the rms value of the output voltage fundamental wave of the HFI, U_{cd} is the rms value of the input voltage of the rectifier bridge of pick-up side, U_R is the load output voltage, I_p and I_s are current rms values of the transmitting and pick-up coil, respectively, L_p, C_p, and R_p are the transmitting side coil self-inductance, compensation capacitance, and transmitting side coil inner resistance, respectively. Besides, L_s, C_s, and R_s are pick-up side coil self-inductance, compensation capacitance, and pick-up side coil inner resistance, respectively, M is the mutual inductance between the transmitting side and the pick-up side coil, C is the output filter capacitor of rectifier bridge of the pick-up side; R is the system load. The system switching frequency is f, and its corresponding cycle time is T, S_1, S_2, S_3, and S_4 are semiconductor switches of the HFI, D_1, D_2, D_3, and D_4 are diodes of pick-up side rectifier.

In the traditional PDM, the output power is regulated by controlling the time $T_{\rm on}$ of the inverter switch to deliver energy to the load within a certain time $T_{\rm all}$. There are N switching cycles in $T_{\rm all}$, in which the power is delivered to the load only during P switching cycles, while the power is not delivered during the remaining N-P switching cycles. The time taken by P switching cycles is $T_{\rm on}$. Therefore, the HFI output voltage is proportional to the pulse density value m that is defined as P/N.

In this article, considering the accuracy of the control, eight switching cycles is used as a PDM control cycle, and P switching cycles of energy transfer are evenly distributed [21]. At the same time, in order to ensure the HFI operates in the ZVS and quasi-ZCS states, one fundamental switching cycle is one resonant cycle. Here, we set $1 \leq N \leq 8$, so that the HFI output voltage has 22 different output voltage values. And if N is only equal to 8, the HFI has only eight different output voltage values.

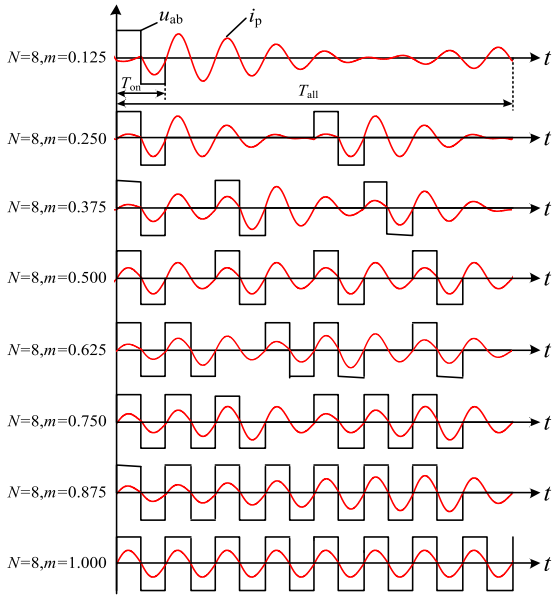

Fig. 2. Output voltage u_{ab} and current i_p of the HFI with different m values of $N = 8$ when using the traditional PDM.

TABLE I
Switching Sequences of the PDM With Different N and m Values

N, m	SW(N, m)	N, m	SW(N, m)
N=8,m=0.125	10000000	N=7,m=0.570	1010101
N=7,m=0.140	1000000	N=5,m=0.600	10101
N=6,m=0.170	100000	N=8,m=0.625	11011010
N=5,m=0.200	10000	N=3,m=0.670	101
N=4,m=0.250	1000	N=7,m=0.710	1110110
N=7,m=0.290	1001000	N=4,m=0.750	1110
N=3,m=0.330	100	N=5,m=0.800	11110
N=8,m=0.375	10100100	N=6,m=0.830	111110
N=5,m=0.400	10100	N=7,m=0.860	1111110
N=7,m=0.430	1010010	N=8,m=0.875	111111110
N=2,m=0.500	10	N=1,m=1.000	1

Fig. 2 shows the HFI output voltage u_{ab} and current i_p with different pulse density m when $N = 8$. Table I lists the traditional PDM with different N values and different pulse density m values, which are represented by the SW(N, m) function. Here, the value 1 represents the switch turn-ON, and 0 means the switch is OFF.

As shown in Fig. 2, when the pulse density is low, the fluctuation of the HFI output current of is large and even a discontinuous current may occur. This will affect the stable operation of the HFI and is not conducive to the implementation of the frequency tracking technology.

III. Analysis of the IPDM Inverter

A. Principle of IPDM

The idea of IPDM technology is to replace the components of the fundamental wave and zero state in the traditional PDM by using harmonics. The switching period of the transmitted energy

TABLE II
SWITCHING SEQUENCES OF THE IPDM WITH DIFFERENT *N* AND *m* VALUES

N, *m*	SW (*N*, *m*)	*N*, *m*	SW (*N*, *m*)
N=8,*m*=0.125	70	*N*=7,*m*=0.570	11310
N=7,*m*=0.140	7	*N*=5,*m*=0.600	131
N=6,*m*=0.170	50	*N*=8,*m*=0.625	113110
N=5,*m*=0.200	5	*N*=3,*m*=0.667	*None*
N=4,*m*=0.250	30	*N*=7,*m*=0.710	11311
N=7,*m*=0.290	330	*N*=4,*m*=0.750	*None*
N=3,*m*=0.333	3	*N*=5,*m*=0.800	*None*
N=8,*m*=0.375	1330	*N*=6,*m*=0.830	*None*
N=5,*m*=0.400	130	*N*=7,*m*=0.860	*None*
N=7,*m*=0.430	133	*N*=8,*m*=0.875	*None*
N=2,*m*=0.500	*None*	*N*=1,*m*=1.000	*None*

can be evenly distributed throughout the IPDM control switching cycle. For example, when $N = 4$, $m = 0.25$, the conventional PDM is composed of one fundamental switching period and three zero-state switching periods. While IPDM is composed of a third harmonic switching period and a zero-state switching period.

A period of harmonics can only be introduced if there is more than one fundamental switching period and a plurality of zero-state switching periods in a total control switching period of the conventional PDM. For instance, one fundamental switching cycle and two zero-state switching cycles can form a third harmonic cycle. And among all harmonic components, the third harmonic accounted for the least number of switching cycles of the fundamental wave. Therefore, when harmonics are introduced in the IPDM, the number of switching periods *P* and the number of total switching periods *N* should satisfy the following relationship:

$$N - P \geq 2. \tag{1}$$

Here, we convert conventional PDM for a certain pulse density *m* into multiple different modulation methods consisting of fundamental, harmonics, and zero states. For example, when $N = 7$, $m = 0.43$, the optimized modulation can be divided into two schemes. Scheme I consists of two fundamental switching periods and one-fifth harmonic switching period. And scheme II consists of one fundamental switching cycle and two-third harmonic switching cycles. Theoretically, it can be seen that the rms values of the HFI output voltage and current of the two modulation methods are consistent. But the output current fluctuation of the scheme I is significantly higher than the scheme II because the scheme I is significantly lower than the scheme II for distribution uniformity of switching cycles transferring energy to the load.

Therefore, when it is to use a combination of fundamental waves or harmonics, we have to follow the principle that only adjacent fundamental and harmonics can be combined, such as fundamental and third harmonic, third harmonic, and fifth harmonics, etc.

According to the IPDM idea and the principle of combination of fundamental, harmonics, and zero state, and judging whether harmonics can be introduced, the modulation results of IPDM are shown in Table II.

TABLE III
MAIN CIRCUIT PARAMETERS OF ICPT SYSTEM

Symbol	Parameter	Value	Unit
U_{dc}	Input DC voltage	300	V
P	Rated output power	20	kW
N	Matching transformer ratio	4:1	
C_0	DC bus supporting capacitor	1000	μF
C_1	DC bus high frequency absorption capacitor	0.22	μF
L_p	Transmitting coil self-inductance	22.14	μH
C_p	Transmitting side compensation capacitance	1270	nF
R_p	Transmitting coil inner resistance	0.033	Ω
L_{s1}	Pick-up coil 1# self-inductance	979	μH
L_{s2}	Pick-up coil 2# self-inductance	982	μH
L_{s3}	Pick-up coil 3# self-inductance	980	μH
L_{s4}	Pick-up coil 4# self-inductance	982	μH
C_s	Pick-up side compensation capacitance	0.03	μF
R_s	Pick-up coil inner resistance	0.492	Ω
M_1	Mutual inductance (transmitting & pick-up coil 1#)	17.2	μH
M_2	Mutual inductance (transmitting & pick-up coil 2#)	17.2	μH
M_3	Mutual inductance (transmitting & pick-up coil 3#)	17.2	μH
M_4	Mutual inductance (transmitting & pick-up coil 4#)	17.3	μH
C	Output capacitance of each pick-up module rectifier	500	μF

1 represents the fundamental switching pulse; 3, 5, and 7 represent the third, fifth, and seventh harmonic switching pulse, respectively; and 0 represents the zero-state switching pulse. *None* means that the corresponding *N* and *m* cannot be achieved by the IPDM.

Compared with the traditional PDM, IPDM can optimize the distribution of *P* switching cycles to reduce current fluctuation, especially at light loads. Therefore, IPDM can be used in the case of light and medium loads.

B. Harmonic Optimization

After phase shifting of each harmonic, the rms value of the HFI output voltage is the same at some phase-shift angles. The phase-shift angle is defined as the angle at which the drive of S4 lags behind S1 in the article. For example, when the phase-shift angles of the fifth harmonic are 0°, 72°, and 144°, respectively, their corresponding HFI output voltages have the same rms value. Therefore, the output current fluctuation with different phase-shift angles is compared to obtain the best phase-shift angle that can achieve the minimum current fluctuation.

Here, we take the fifth-order harmonic as an example. In order to achieve soft switching and the output voltage constant after phase shift, the angle can only be 0°, 72°, and 144°. Fig. 3 shows the HFI output voltage and current waveforms and IGBT drive signals for the fifth harmonic after phase shifting (HAPS). The output currents of these three phase-shift angles are analyzed.

The HFI output current $i_p(t)$ is expressed as follows:

$$L[i_p(t)] = F(s)\left[L[u(t)] + L_p i_p(0_-) + L[u_{Cp}(0_-)]\right] \tag{2}$$

where *F*(s) is the transfer function of the ICPT system, *u*(*t*) is the output voltage of HFI, $i_p(0-)$ and $u_{Cp}(0-)$ coil initial current and compensation capacitor initial voltage. L[ ] is a Laplace operator.

1) Phase-shift angle 0°: during t_0 to t_5, $u_{Cp}(t) = C_p di_p/dt + v$ since the transmitting side compensation capacitor has the function of isolating dc voltage. To simplify the analysis, it is assumed that the voltage

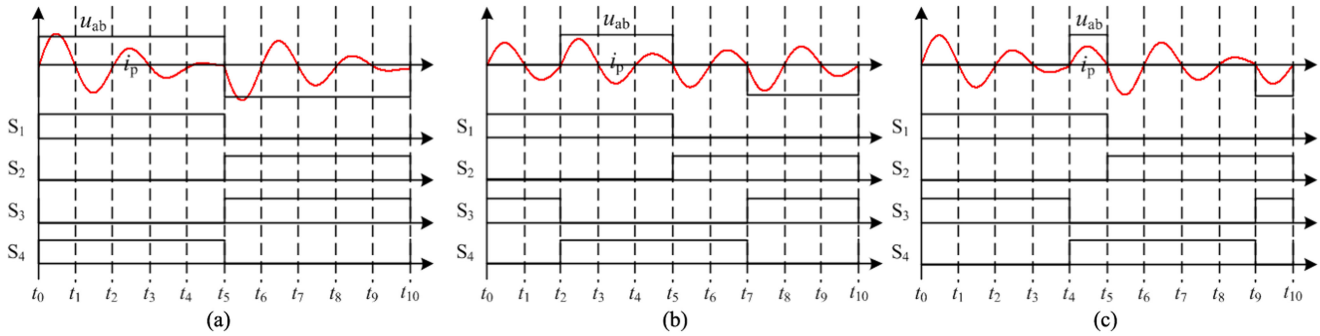

Fig. 3. HFI output voltage and current and IGBT drive waveforms for the fifth harmonic at different phase-shift angles. (a) 0°. (b) 72°. (c)144°.

component v of the resonant capacitor can be stabilized to $U_{\rm dc}$ in half a resonant period. Once the HFI output voltage changes, the voltage v will be released and the output current will increase. And it is assumed that it will only affect the current fluctuation of the half of the resonance period. Therefore, the change in current can be divided into two processes within the half of the IPDM control cycle.

In $t_0 \sim t_1$, $u(t) = U_{\rm dc}$, $i_p(0_-) = 0$, $u_{Cp}(0_-) = f(I_p) + v$, and $v = U_{\rm dc}$, the current is in full state response and the peak value of the current increases due to the influence of $u(t)$ and v. In $t_1 \sim t_5$, $u(t) = U_{\rm dc}$, $i_p(0_-) = 0$, $u_{Cp}(0_-) = f(I_p) + v$, and $v = U_{\rm dc}$, $f(I_p) = \sqrt{2} I_p / \omega C_p$, the current is in a freely attenuated state. The current in $t_5 \sim t_{10}$ can be analyzed by the same method, and the result is consistent with that in $t_0 \sim t_5$.

2) Phase-shift angle 72°: the current change can be divided into four processes within the half of the IPDM control cycle. In $t_0 \sim t_1$, $u(t) = 0$, $i_p(0_-) = 0$, $u_{Cp}(0_-) = f(I_p) + v$, and $v = U_{\rm dc}$, the peak value of the current increases due to the influence of v. In $t_1 \sim t_2$, $u(t) = 0$, $i_p(0_-) = 0$, $u_{Cp}(0_-) = f(I_p) + v$, and $v = 0$, the current is in a freely attenuated state. In $t_2 \sim t_3$, $u(\mathrm{t}) = U_{\rm dc}$, $i_p(0_-) = 0$, $u_{Cp}(0_-) = f(I_p) + v$, and $v = 0$, the current is in full state response and the peak value of the current increases due to the influence of $u(t)$. In $t_3 \sim t_5$, $u(t) = U_{\rm dc}$, $i_p(0_-) = 0$, $u_{Cp}(0_-) = f(I_p) + v$, and $v = -U_{\rm dc}$, the current is in a freely attenuated state.

3) Phase-shift angle 144°: the current change is divided into three processes within the half of the IPDM control cycle. In $t_0 \sim t_1$, $u(t) = 0$, $i_p(0_-) = 0$, $u_{Cp}(0_-) = f(I_p) + v$, and $v = U_{\rm dc}$, the peak value of the current increases due to the influence of v. In $t_1 \sim t_4$, $u(t) = 0$, $i_p(0_-) = 0$, $u_{Cp}(0_-) = f(I_p) + v$, and $v = 0$, the current is in a freely attenuated state. In $t_4 \sim t_5$, $u(\mathrm{t}) = U_{\rm dc}$, $i_p(0_-) = 0$, $u_{Cp}(0_-) = f(I_p) + v$, and $v = 0$, the current is in full state response and the peak value of the current increases due to the influence of $u(t)$.

According to the analysis above, it is obtained that the current trend can be divided into multiple rising and falling processes during an IPDM control period. For example, when the phase-shift angle is 0°, the current can be divided into two rising processes and two falling processes, wherein t_0 to t_1 and t_5 to t_6 are rising processes, and t_1 to t_5 and t_6 to t_{10} are falling processes. Similarly, when the phase-shift angle is 72° and 144°, the current can be divided into four rising processes and four falling processes, and two rising processes and two falling processes, respectively.

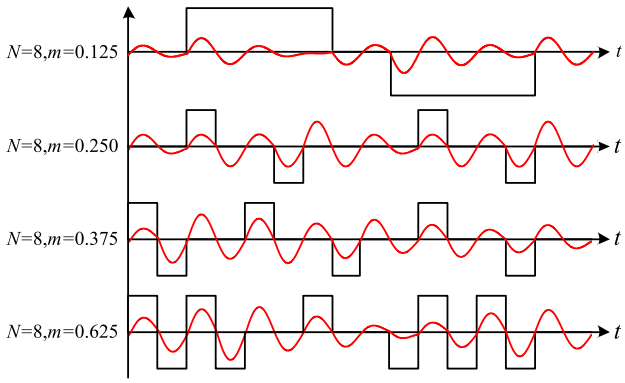

Fig. 4. HFI output voltage and current with different pulse density m of $N = 8$ when using IPDM.

Since the rms values of the output current are equal in the three phase-shift angles in one IPDM period, the more the number of rising and falling processes in which the current is divided, the smaller the fluctuation of the current. Finally, the fifth harmonic with 72° phase-shift angle can minimize output current fluctuation.

Through a similar current response process analysis method, the phase-shift angles of the third harmonic and the seventh harmonic can be selected to be 120° and 77°, respectively.

Fig. 4 shows that the HFI output voltage and current waveforms of different pulse density numbers with IPDM when $N = 8$. It can be seen that the proposed IPDM further optimizes the distribution of P switching cycles, thereby reducing the output current fluctuation of the HFI.

C. Switching Scheme and ZVS

According to the current flow direction and switching state, six switching modes of the HFI are obtained. Fig. 5 shows the equivalent circuit of transmitting side with six switching modes. From the view of whether the power source transfers energy to the load, mode I and mode II can be collectively referred to as "active mode," and mode III and mode IV can be collectively

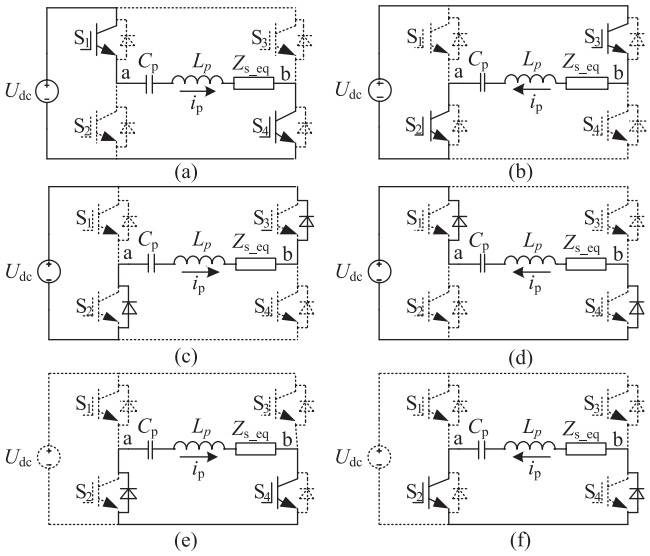

Fig. 5. Equivalent circuit of transmitting side and six switching modes. (a) Mode I. (b) Mode II. (c) Mode III. (d) Mode IV. (d) Mode V. (f) Mode VI.

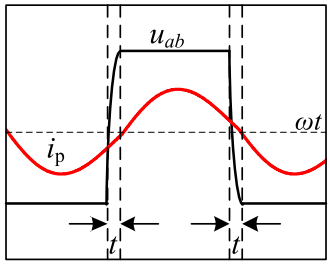

Fig. 6. Output voltage and current waveforms of HFI.

referred to as "brake mode," and mode V and mode VI can be collectively referred to as "zero-state mode."

The output voltage and current waveforms with dead time of HFI are shown in Fig. 6. t is the time occupied by the output voltage from negative (positive) to positive (negative). It is necessary to keep the output current negative (positive) during the process. The t can be calculated according to the analysis of charge and discharge.

It is clearly that the current in the resonant circuit must be large enough to change the voltage of HFI to $U_{\rm dc}$ or $-U_{\rm dc}$ before the current crosses zero.

$$t = \frac{1}{\omega}\cos^{-1}\left(1 - \frac{2\omega C_e U_{\rm dc}}{I_p}\right) \tag{3}$$

where ω is the angular frequency corresponding to HFI switching frequency, C_e is the equivalent capacitance of HFI (the parasitic capacitance and absorption capacitance of IGBT), $U_{\rm dc}$ is the voltage of the dc link, and I_p is the output current rms value of HFI.

Therefore, the calculated t value can be used as the minimum dead time t_d of the IGBT in order to ensure ZVS.

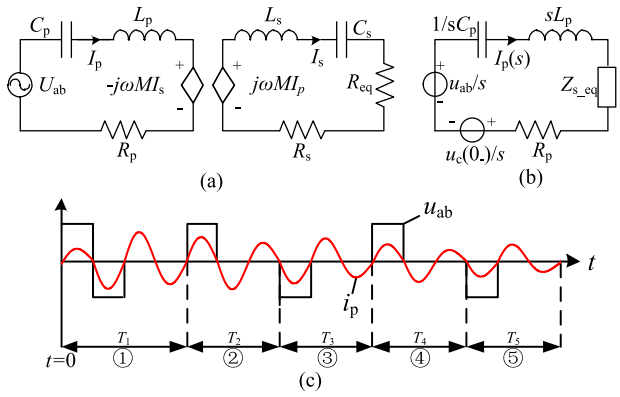

Fig. 7. Equivalent circuit of the ICPT system and the HFI output voltage and current waveforms when $N = 8$ and $m = 0.375$.

D. Analysis of the Output Current Ripple of the HFI

Fig. 7(a) shows the equivalent circuit of the ICPT system, Fig. 7(b) shows the complex frequency domain circuit on the transmitting side of the ICPT system, and Fig. 7(c) shows the HFI output voltage and current waveforms when $m = 0.375$.

In order to analyze the fluctuation of the output current, it is necessary to subdivide the current of one IPDM control switching cycle into multiple subprocesses. Each adjacent rising and falling process of the output current peak is defined as a subprocess. As can be seen from the Fig. 7(c), the whole process can be subdivided into five subprocesses during an IPDM control switching cycle. The switching time of these five subprocesses is T_1 to T_5, respectively.

The steady-state system can be described by the following equations according to Fig. 7(a) and the KVL:

$$\begin{cases} U_{ab} = (j\omega L_p + \frac{1}{j\omega C_p} + R_p)I_p - j\omega M I_s \\ 0 = (j\omega L_s + \frac{1}{j\omega C_s} + R_s + R_{eq})I_p + j\omega M I_p \end{cases} \tag{4}$$

where ω is equal to the resonant frequency of the system, and $R_{\rm eq}$ is the ac equivalent resistance of the pick-up side.

When both the transmitting side and the pick-up side are in full resonance state, the impedance of the pick-up side reflected to the transmitting side can be expressed as

$$Z_{s\_\rm eq} = \frac{(\omega M)^2}{R_{\rm eq} + R_s}. \tag{5}$$

Here, subprocess 1 is considered as an example. According to KVL combined with Fig. 7(b), the following equation of the transmitting side is obtained:

$$\frac{u_{ab} - u_c(0_-)}{s} = I_p(s)\left(sL_p + \frac{1}{sC} + R_p + Z_{s\_\rm eq}\right). \tag{6}$$

The transmission side quality factor $Q_p = 2\omega L_p/(R_p + Z_{s\_\rm eq})$, assuming $Q_p \gg 1$, the transmitting coil current is given by

$$i_p(t) = i_{E,1}\sin(\omega t). \tag{7}$$

$i_{E,1}$ is the peak envelope of the output current of the HFI during subprocess 1. When $t = 0$, $T/2$, and T, the initial voltage of the compensation capacitor is x_1, x_2, and x_3. $i_{E,1}$ can be

written as

$$i_{E,1}(t)=\begin{cases}\dfrac{U_{\rm dc}-x_1}{\omega L{\rm p}}e^{\frac{t}{-\tau}} & 0\le t\le T/2\\ \dfrac{-U_{\rm dc}-x_2}{\omega L{\rm p}}e^{\frac{t-T/2}{-\tau}} & T/2\le t\le T\\ \dfrac{-x_3}{\omega L{\rm p}}e^{\frac{t-T}{-\tau}} & T\le t\le 2T\end{cases}\tag{8}$$

where $\tau=2L_p/(Z_{s\_\rm eq}+R_p)$.

According to the relationship between the capacitor voltage and current, the capacitor C_p voltage can be derived as eq. (9) shown at the bottom of this page.

Since $u_{c,1}(0)=x_1$, $\rm A_1$ can be expressed as

$$A_1=\frac{\omega L_pC_px_1}{U_{\rm dc}-x_1}-1.\tag{10}$$

Similarly, x_2, x_3, $\rm A_2$, and $\rm A_3$ can all be represented by x_1. Also, due to $u_{c,5}(8T)=u_{c,1}(0)=x_1$, x_1 can be solved. The current expression for the entire process can be derived, then the maximum value $i_{E\_\max}$ and minimum value $i_{E\_\min}$ of the current peak are obtained. The output current peak-to-peak value ripple in one IPDM control period can be expressed as

$$\Delta I=i_{E\_\max}-i_{E\_\min}.\tag{11}$$

It is distinct the maximum of the current peak is related to the time taken by the "active mode" during each subprocess, and the longer the time, the larger the maximum of the current peak.

Similarly, the longer the time occupied by the passive mode, the smaller the minimum value of the current peak. Therefore, $i_{E\_\min}$ is 0 for both PDM and IPDM. Comparing the pulse distributions of PDM in Table I and IPDM in Table II, it can be seen that the time taken by the "active mode" of IPDM is less than PDM during each subprocess for output power lower than 16% of the rated power ($N=5$, $m=0.4$), then $i_{E\_\max}$ of IPDM is less than that of PDM. Finally, the proposed IPDM can reduce HFI output current fluctuation.

E. Output Power and System Efficiency

The rms value of the HFI output voltage and output power can be expressed as

$$\begin{cases}U_{ab}=m\dfrac{2\sqrt{2}U_{\rm dc}}{\pi}=\dfrac{2\sqrt{2}U_{\rm dc}}{\pi}\dfrac{T_{\rm on}}{T_{\rm all}}\\ P_o=\dfrac{U_{ab}^2}{Z_{\rm eq}}=\dfrac{8U_{\rm dc}^2}{\pi^2Z_{\rm eq}}\left(\dfrac{T_{\rm on}}{T_{\rm all}}\right)^2=P_{\max}\left(\dfrac{T_{\rm on}}{T_{\rm all}}\right)^2\end{cases}\tag{12}$$

where $P_{\max}$ is the HFI output power for $T_{\rm on}/T_{\rm all}=1$.

From Fig. 7(c), an IPDM control cycle can be subdivided into multiple subprocesses. These subprocesses are mainly composed of switching cycles of fundamental, HAPS and zero state. In order to simplify the analysis, this article does not consider the case of harmonics above seventh harmonic. Therefore, in an IPDM control period T, T_{1f} and T_0 are set to the time of the fundamental and zero-state switching cycles, respectively, and the time of the third, fifth, and seventh HAPS switching cycles is $T_{\rm 3rd}$, $T_{\rm 5th}$, and $T_{\rm 7th}$, respectively. Therefore, according to (12), the average output power of an entire IPDM control cycle is

$$P_o=P_{\max}\left(\frac{T_{1f}+T_{\rm 3rd}/3+T_{\rm 5th}/5+T_{\rm 7th}/7}{T_{\rm all}}\right)^2.\tag{13}$$

According to the above analysis, it is clear that the output power can be adjusted by simply adjusting the time occupied by the switching cycles of fundamental, harmonics, and zero state.

Since the time of an IPDM control cycle is $T_{\rm all}$ and the corresponding frequency is $f_{\rm all}$. Using $f_{\rm all}$ as the fundamental wave, performing Fourier decomposition on HFI output voltage within one control cycle, the HFI output voltage can be expressed as

$$\begin{aligned}u_{ab}(t)=&\,u_1\sin(\omega_1t+\varphi_1)+u_2\sin(\omega_2t+\varphi_2)\\&+\cdots+u_n\sin(\omega_nt+\varphi_n)\end{aligned}\tag{14}$$

where $n\in N$, $\omega_1=2\pi f_{\rm all}$. $\omega_n=n\omega_1$.

According to (14), the transmitting coil and pick-up coil current can be expressed as

$$\begin{cases}i_p(t)=\sum_{i=0}^{n}u_i\dfrac{Z_{s(i)}}{(\omega_iM)^2+Z_{p(i)}Z_{s(i)}}\sin(\omega_it+\varphi_i)\\ i_s(t)=\sum_{i=0}^{n}u_i\dfrac{j\omega_iM}{(\omega_iM)^2+Z_{p(i)}Z_{s(i)}}\sin(\omega_it+\varphi_i-\pi/2)\end{cases}\tag{15}$$

where $Z_{p(i)}=j(\omega_iL_p-1/\omega_iC_p)+R_p$, $Z_{s(i)}=\rm j(\omega_iL_s-1/\omega_iC_s)+R_s+R_{eq}$, $\rm i=1, 2, \ldots, \it n$.

Regardless of used modulation strategy, the components of the HFI output voltage at the switching frequency point are equal when the pulse densities are equal. The corresponding current components are also equal.

It is easy to know that the component of the HFI output current at other frequency points is related to the magnitude of the current ripple. And the greater the fluctuation of the current is, the larger the current component of other frequencies. In other words, the greater the current fluctuation, the greater the inverter loss, the inner resistance loss of the transmitting coil and pick-up coils.

$$u_{c,1}(t)=\begin{cases}\dfrac{U_{\rm dc}-x_1}{\omega L_pC_p}\left(e^{\frac{t}{-\tau}}\sin\left(\omega t-\dfrac{\pi}{2}\right)+A_1\right) & 0\le t\le T/2\\ \dfrac{U_{\rm dc}+x_2}{-\omega L_pC_p}\left(e^{\frac{t-T/2}{-\tau}}\sin\left(\omega\left(t-\dfrac{T}{2}\right)-\dfrac{\pi}{2}\right)+A_2\right) & T/2\le t\le T\\ \dfrac{-x_3}{\omega L_pC_p}\left(e^{\frac{t}{-\tau}}\sin\left(\omega(t-T)-\dfrac{\pi}{2}\right)+A_3\right) & T\le t\le 2T\end{cases}\tag{9}$$

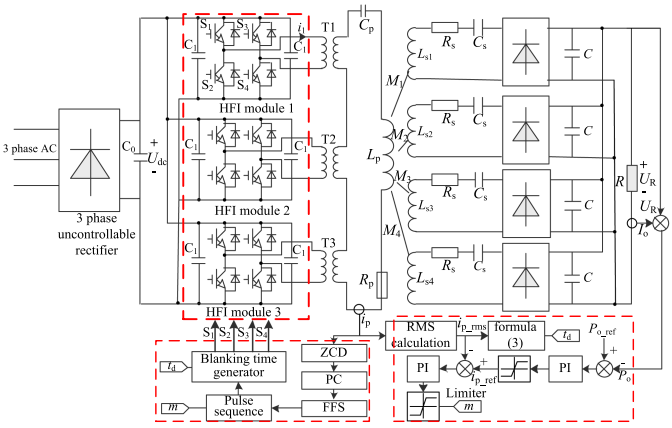

Fig. 8. Schematic diagram of the tuning method and closed-loop control of output power.

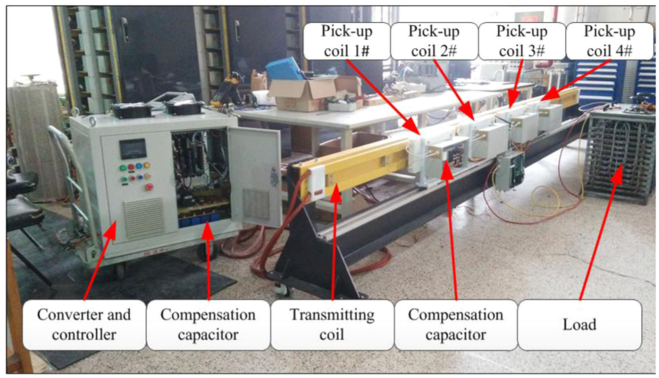

Fig. 9. Prototype of ICPT system developed by our laboratory.

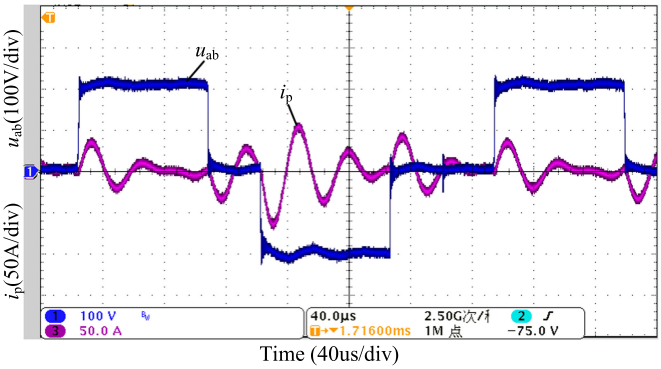

Fig. 10. Experimental waveforms of the output voltage and current of HFI using IPDM for 1.5% of the rated output power.

Therefore, IPDM can not only reduce HFI output current fluctuation, but also improve system efficiency.

IV. Control Strategy

In order to ensure the ZVS implementation of the HFI and the stable control of the output voltage, the tuning method and closed-loop control of output power are established, as shown in Fig. 8. The control scheme can be divided into the following two parts:

1) A dual closed-loop control strategy is applied. The load power and the primary current are controlled as outer and inner loops, respectively. The dual PI closed-loop control strategy can prevent the excessive current on the transmitting side caused by the fault of the closed-loop power control. The output of the double closed-loop control algorithm is the pulse density number and is sent to the Field Programmable Gate Array (FPGA) for generating the drive signal. The dead time is used to prevent the two switches of one bridge from being turned ON at the same time to cause a short circuit problem. The dead time can be calculated by equation (3).
2) A tuning method based on current zero crossing detection (ZCD) and phase comparison (PC) is applied. First, a fixed frequency signal (FFS) is generated. Second, PC can be performed between the FFS and the high-frequency signal generated by the current ZCD. If the phase angle difference is less than the phase angle corresponding to the dead time, frequency is adjusted until ZVS is achieved. This FFS is used as a reference for forming the drive signal. The dead time is set to 1 μs.

It can be calculated that there are different ZVS frequency points for different loads. In order to prevent the ZVS frequency from deviating significantly from resonance point, the frequency is limited to 29∼30 kHz.

Finally, the pulse sequence is determined by the FFS and switch sequences of the pulse density m. Switch sequence can be obtained by looking up the table. The FPGA completes the generation of the pulse signal to ensure the synchronization of the signal.

V. Experimental Verification

A. Prototype Setup

A prototype of ICPT system developed in our Lab. for medium speed maglev train is shown in Fig. 9. Table III is the prototype parameters. The transmitting side is composed of three-phase uncontrolled rectifier, three sets of full-bridge HFI, and two matching transformers. The pick-up side system includes four parallel pick-up modules and uncontrolled rectifiers that supply power to the load. The solution of laying magnetic cores on the long-segment transmitting coil is not considered because of cost. The transmitting coil along the track has two turns with no ferrite core. In order to increase the coupling coefficient, the magnetic core on the pick-up is arranged in a spaced manner. In addition to the modulation strategy, quality factor is an important parameter that affects the HFI output current ripple. Therefore, a constant load $R = 6\ \Omega$ is used to keep the quality factor constant during experiment.

B. Output Current Ripple

Figs. 10–13 show experimental waveforms of the HFI output voltage u_{ab} and current i_p when using IPDM with different pulse

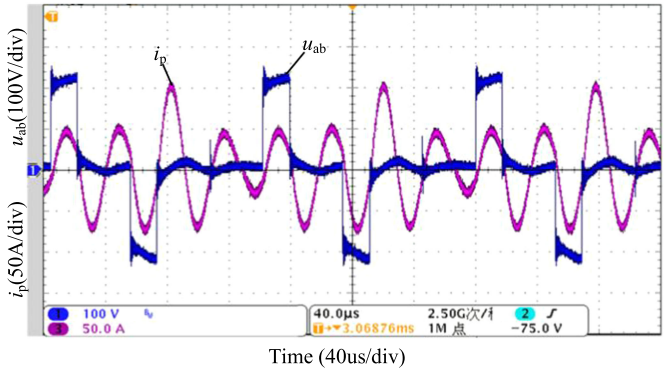

Fig. 11. Experimental waveforms of the output voltage and current of HFI using IPDM for 6.25% of the rated output power.

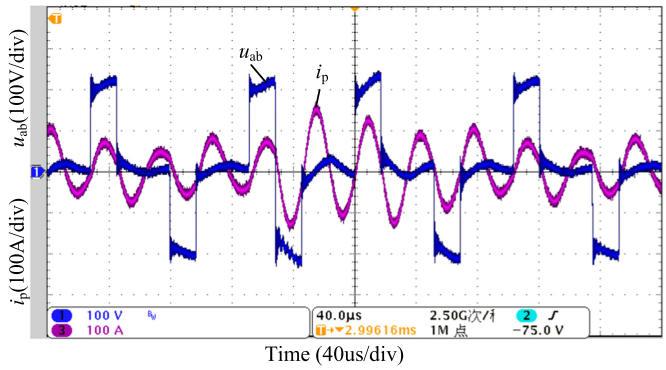

Fig. 12. Experimental waveforms of the output voltage and current of HFI using IPDM for 14.1% of the rated output power.

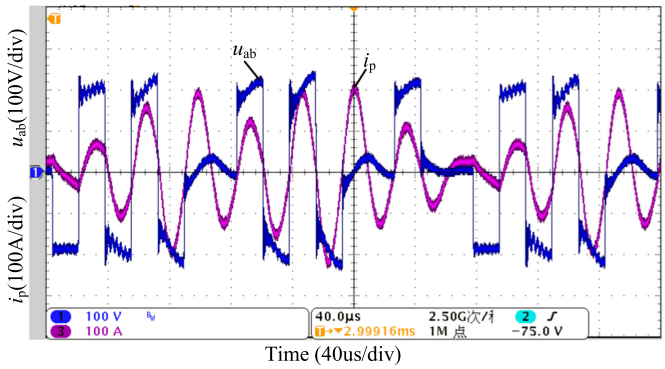

Fig. 13. Experimental waveforms of the output voltage and current of HFI using IPDM for 39% of the rated output power.

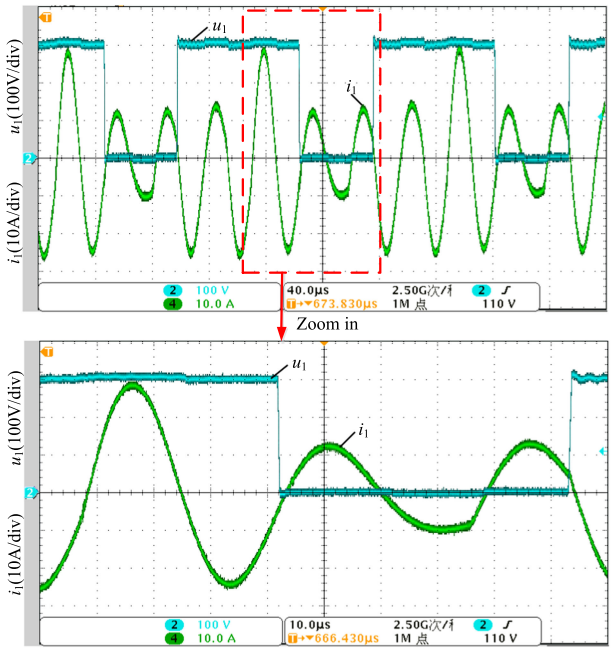

Fig. 14. Details of the ZVS process for 6.25% of the rated output power.

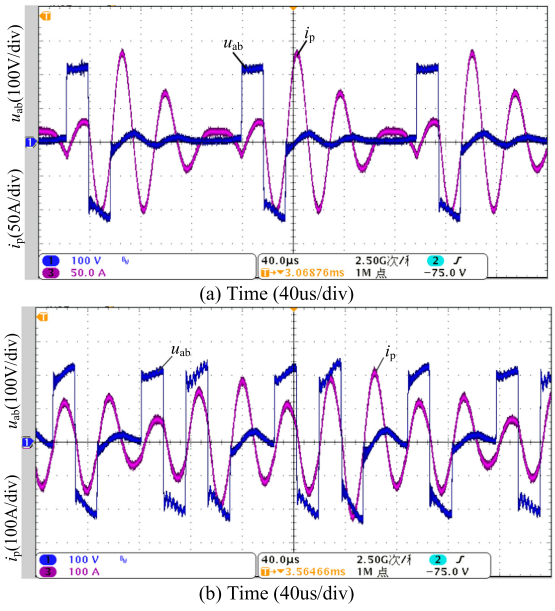

Fig. 15. Experimental waveforms of the output voltage and current of HFI using PDM for (a) 6.25% and (b) 39% of the rated output power.

density numbers at $N = 8$. Their corresponding output powers range are from 0.3 to 8 kW (1.5%, 6.25%, 14.1%, and 39% of the rated output power), respectively.

Fig. 14 shows the detailed switching process of the HFI for 6.25% of the rated output power. u_1 and i_1 are the voltage across the switch S_1 and the output current of the HFI module 1, respectively. As shown in Fig. 14, the ZVS of the HFI is implemented at turn-ON to increase the HFI efficiency.

As can be seen from Figs. 11 and 13, the maximum and minimum current peak values are 102 and 35 A, 205 and 40 A in one IPDM cycle, respectively, then $\Delta I = 67$ A and $\Delta I = 165$ A. Fig. 15 shows the output voltage and current waveforms of HFI with PDM when $N = 8$, $m = 0.25$, and $m = 0.625$ (6.25% and 39% of the rated output power). The maximum and minimum current peak values are 135 and 15A, 212 and 77A in one PDM cycle, respectively, then $\Delta I = 120$ A and $\Delta I = 135$ A. By comparing the output current waveforms in Fig. 16, the proposed IPDM can reduce the output current ripple and solves the current

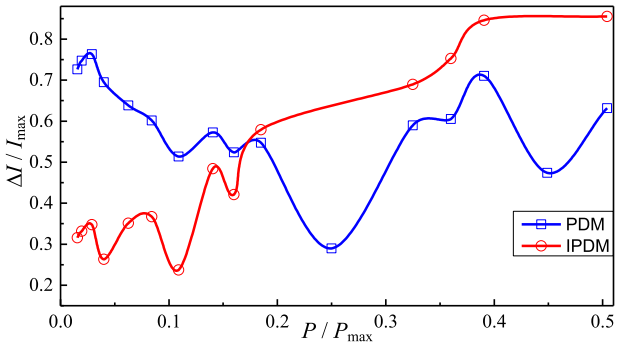

Fig. 16. Normalized peak-to-peak ripple coefficient of the output current at different output power when using PDM and IPDM.

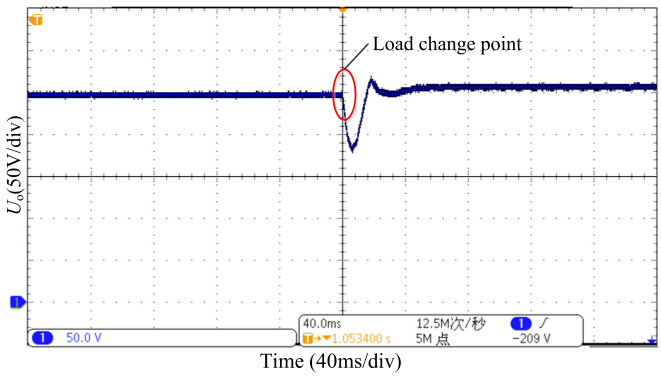

Fig. 17. Output voltage waveform as load changed from 36 to 6 Ω.

discontinuity problem at light load. Conversely, the HFI output current fluctuation of the PDM is smaller than the IPDM at middle or heavy load.

Fig. 16 shows the normalized peak-to-peak ripple coefficient with respect to the output current maximum $I_{\max}$ at different output power by using PDM and IPDM. It is known from Fig. 16, the output current ripple coefficient is reduced by 15% to 62% for output power lower than 16% with IPDM compared to PDM. Especially for output power lower than 11%, the output current ripple coefficient is reduced by 39% to 62%.

Although the IPDM can also be applicable to some medium load conditions, the current ripple coefficient will increase. The main reason is that the introduction of harmonics reduces the uniformity of the distribution of the switch sequence.

Therefore, the proposed IPDM is better applicable to light loads. When $m \geq 0.4$ (16% of rated output power), PDM is more feasible.

To illustrate that a hybrid modulation strategy combining IPDM and PDM can be used to control the output voltage or power, an experiment was performed in which the load was switched from 36 to 6 Ω. The output voltage is maintained at 250 V by controlling the pulse density m. Fig. 17 shows the output voltage waveform as load changed. Fig. 18 shows the HFI output voltage and current waveforms before and after load switching.

It can be seen that the stability of the output voltage can be achieved by closed loop control. IPDM with $m = 0.14$ is used for $R = 36$ Ω and PDM with $m = 0.71$ is used for $R = 6$ Ω. In other words, it is possible to use IPDM at light load and PDM at heavy load.

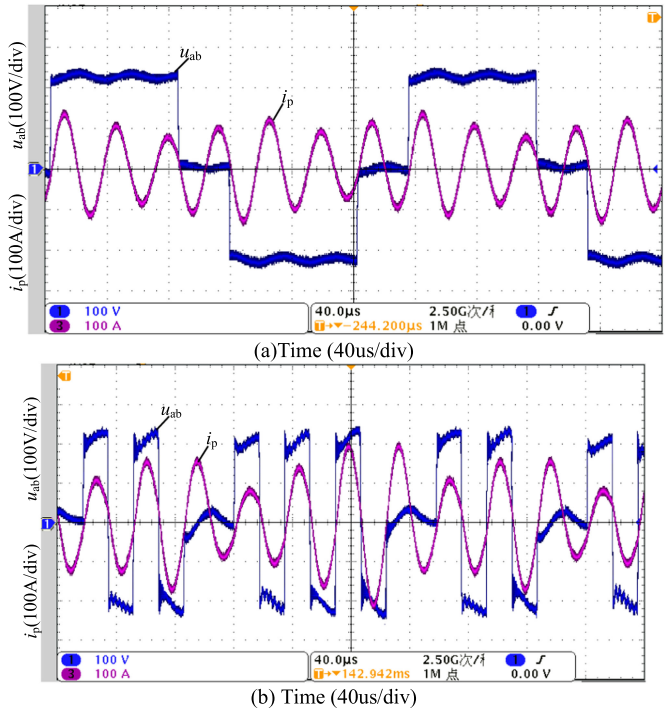

Fig. 18. HFI output voltage and current waveforms (a) before and (b) after load switching.

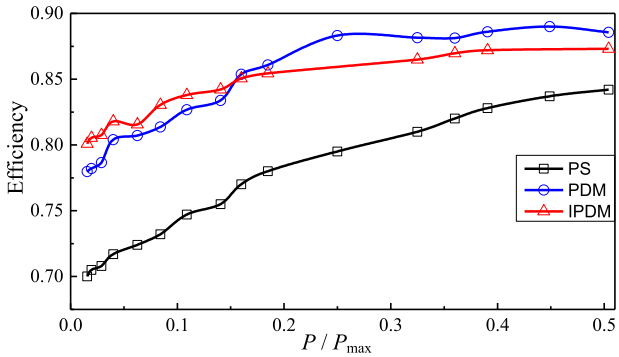

Fig. 19. System efficiency cures with three different modulation strategies.

C. System Efficiency

Here, the efficiency of measurement and calculation is from the three-phase grid side to the load side. The systematic efficiency comparison is conducted among PS, PDM, and IPDM.

Fig. 19 shows the system efficiency curves versus the normalized output power for three modulation strategies. It can be seen the system efficiency of PS is significantly smaller than PDM and IPDM at the light and middle load, and the system efficiency becomes low as the output power is decreased. The

main reason is that the PS inverter cannot achieve ZVS at turn ON. Both PDM and IPDM can achieve ZVS regardless of light or middle load. At the same time, the system efficiency of IPDM has been improved compared with PDM at light load because IPDM significantly reduces the output current fluctuation. It is consistent with the theoretical analysis.

VI. Conclusion

A proposed novel IPDM based on harmonics is feasible to reduce the HFI output current ripple and improve system efficiency at the light load. Conversely, PDM is more suitable for medium or heavy load. Load change experiment verified that voltage control can be achieved using PDM and IPDM in combination. And a comparison experiment about the ripple coefficient of the output current and the system efficiency was studied among PS, PDM, and IPDM. IPDM has the following advantages at light load:

1) The ripple coefficient of IPDM output current is reduced by 15% to 62% compared to PDM at light load.
2) The IPDM has the best efficiency among PS, PDM, and IPDM.

References

[1] J. T. Boys, G. A. Covic, and A. W. Green, "Stability and control of inductively coupled power transfer systems," *IEE Proc. Elect. Power Appl.*, vol. 147, no. 1, pp. 37–43, Jan. 2000.

[2] N. A. Keeling, G. A. Covic, and J. T. Boys, "A unity-power-factor IPT pickup for high-power applications," *IEEE Trans. Ind. Electron.*, vol. 57, no. 2, pp. 744–751, Feb. 2010.

[3] W. Zhong, C. K. Lee, and S. Y. R. Hui, "General analysis on the use of tesla's resonators in domino forms for wireless power transfer," *IEEE Trans. Ind. Electron.*, vol. 60, no. 1, pp. 261–270, Jan. 2013.

[4] G. A. Covic and J. T. Boys, "Modern trends in inductive power transfer for transportation applications," *IEEE J. Emerg. Sel. Topics Power Electron.*, vol. 1, no. 1, pp. 28–41, Mar. 2013.

[5] S. Jeong, Y. J. Jang, and D. Kum, "Economic analysis of the dynamic charging electric vehicle," *IEEE Trans. Power Electron.*, vol. 30, no. 11, pp. 6368–6377, Nov. 2015.

[6] C.-G. Kim, D.-H. Seo, J.-S. You, J.-H. Park, and B.-H. Cho, "Design of a contactless battery charger for cellular phone," *IEEE Trans. Ind. Electron.*, vol. 48, no. 6, pp. 1238–1247, Dec. 2001.

[7] J. H. Kim *et al.*, "Development of 1-MW inductive power transfer system for a high-speed train," *IEEE Trans. Ind. Electron.*, vol. 62, no. 10, pp. 6242–6250, Oct. 2015.

[8] L. Jiang, L. Shi, M. Fan, F. Zhang, and Y. Li, "Segment control scheme of inductive power transfer system for rail transit," *IEEE Trans. Ind. Appl.*, vol. 54, no. 4, pp. 3271–3280, Jul./Aug. 2018.

[9] P. Wu, L. Shi, H. Cai, and Y. Li, "An inductively coupled power transfer system based power control for motor drives of rail transit vehicle," in *Proc. 17th Int. Conf. Elect. Mach. Syst.*, 2014, pp. 202–205.

[10] J. G. Bum and B. H. Cho., "An energy transmission system for an artificial heart suing leakage inductance compensation of transcutaneous transformer," *IEEE Trans. Power Electron.*, vol. 13, no. 6, pp. 1013–1022, Nov. 1998.

[11] M. Fan *et al.*, "A novel pulse density modulation with semi-bridgeless active rectifier in inductive power transfer system for rail vehicle," *CES Trans. Elect. Mach. Syst.*, vol. 1, no. 4, pp. 397–404, Dec. 2017.

[12] K. Colak, M. Bojarski, E. Asa, and D. Czarkowski, "A constant resistance analysis and control of cascaded buck and boost converter for wireless EV chargers," in *Proc. IEEE Appl. Power Electron. Conf. Expo.*, 2015, pp. 3157–3161.

[13] E. Gati, G. Kampitsis, and S. Manias, "Variable frequency controller for inductive power transfer in dynamic conditions," *IEEE Trans. Power Electron.*, vol. 32, no. 2, pp. 1684–1696, Feb. 2017.

[14] Y. Li, R. Mai, L. Lu, T. Lin, Y. Liu, and Z. He, "Analysis and transmitter currents decomposition based control for multiple overlapped transmitters based WPT systems considering cross couplings," *IEEE Trans. Power Electron.*, vol. 33, no. 2, pp. 1829–1842, Feb. 2018.

[15] J. Hou *et al.*, "Analysis and control of S/SP compensation contactless resonant converter with constant voltage gain," in *Proc. IEEE Energy Convers. Congr. Expo.*, 2013, pp. 2552–2558.

[16] J. M. Miller, C. P. White, O. C. Onar, and P. M. Ryan, "Grid side regulation of wireless power charging of plug-in electric vehicles," in *Proc. IEEE Energy Convers. Congress Expo.*, Raleigh, NC, USA, 2012, pp. 261–268.

[17] J. M. Miller, O. C. Onar, and M. Chinthavali, "Primary-side power flow control of wireless power transfer for electric vehicle charging," *IEEE J. Emerg. Sel. Topics Power Electron.*, vol. 3, no. 1, pp. 147–162, Mar. 2015.

[18] S. Ryu, D. Kim, M. Kim, J. Kim, and B. Lee, "Adjustable frequency–duty-cycle hybrid control strategy for full-bridge series resonant converters in electric vehicle chargers," *IEEE Trans. Ind. Electron.*, vol. 61, no. 10, pp. 5354–5362, Oct. 2014.

[19] W. P. Choi *et al.*, "Comparative study on power conversion methods for wireless battery charging platform," in *Proc. 14th Int. Power Electron. Motion Control Conf.*, Ohrid, North Macedonia, 2010, pp. S15–9–S15–16.

[20] H. Cai, L. Shi, and Y. Li, "Harmonic-based phase-shifted control of inductively coupled power transfer," *IEEE Trans. Power Electron.*, vol. 29, no. 2, pp. 594–602, Feb. 2014.

[21] V. Esteve *et al.*, "Using pulse density modulation to improve the efficiency of IGBT inverters in induction heating applications," in *Proc. IEEE Power Electron. Specialists Conf.*, 2007, pp. 1370–1373.

[22] H. Li, J. Fang, S. Chen, K. Wang, and Y. Tang, "Pulse density modulation for maximum efficiency point tracking of wireless power transfer systems," *IEEE Trans. Power Electron.*, vol. 33, no. 6, pp. 5492–5501, Jun. 2018.

[23] H. Li, S. Chen, J. Fang, Y. Tang, and M. A. de Rooij, "A low-subharmonic, full-range, and rapid pulse density modulation strategy for ZVS full-bridge converters," *IEEE Trans. Power Electron.*, vol. 34, no. 9, pp. 8871–8881, Sep. 2019.

[24] F. Zhang, L. Shi, Z. Yin, M. Fan, and L. Jiang, "Current balance control strategy for inductively coupled power transfer system with parallel pickup modules," in *Proc. IEEE Transp. Electrific. Conf. Expo.*, 2017, pp. 1–6.

Xuerui Sheng received the B.S. degrees in electrical engineering from the North University of China, Taiyuan, China, in 2016. He is currently working toward the Ph.D. degree in electrical engineering with the Institute of Electrical Engineering, Chinese Academy of Sciences, Beijing, China.

His research interests include inductive power transfer system for railway transit and control of high power inductive power transfer system.

Liming Shi (M'12) received the M.S. degree in electrical engineering from the Graduate School of Chinese Academy of Sciences, Beijing, China, in 1990, and the Ph.D. degree in electrical engineering from Kyushu University, Fukuoka, Japan, in 1998.

From 1998 to 2000, he was a Postdoctoral Research Fellow with Japan Society for the Promotion of Sciences, Tokyo, Japan. From 2000 to 2002, he was the Chief Researcher with Yaskawa Electric Company, Ltd., Kitakyushu, Japan. In 2002, he was with the Institute of Electrical Engineering, Chinese Academy of Sciences, Beijing, China, where he is currently a Professor.

His research interests include analysis and control of electrical machines and wireless power transfer technology.